

The atmospheric corrosion of statue bronzes exposed to SO₂ and NO₂

Die atmosphärische Korrosion von Statuenbronzen bei Anwesenheit von SO₂ und NO₂

H. Strandberg*, L.-G. Johansson and O. Lindqvist

We report on the atmospheric corrosion of different cast statue bronzes in humid air containing ppb levels of SO₂ and SO₂+NO₂. In addition, copper, tin, zinc, and lead samples were studied in these environments. The samples were exposed to synthetic atmospheres with careful control of pollutant concentrations, relative humidity and flow conditions. Deposition of SO₂ was studied using on-line gas analysis. The weight gain was registered after four weeks exposure, and corrosion products were analysed by Electron Probe Micro Analyser (EPMA), X-ray diffraction (XRD), and Fourier Transform Infrared spectroscopy (FTIR).

The synergistic effect of SO₂ and NO₂ was remarkable on all bronze materials examined. The weight gain was correlated to alloy composition. Thus, high zinc and low lead content resulted in the greatest weight gain, while high tin content favoured a low weight increase. Lead exhibited a rapid deposition of SO₂ followed by zinc and copper, while tin was unreactive towards SO₂. There was no measurable indication that microstructure influenced corrosion.

The corrosion product morphology found in SO₂+NO₂ environment indicated a localised type of attack. The anodic sites were covered by a tin-rich corrosion product close to the metal. Oxidation of soluble divalent tin by O₂ at the anodic sites to form insoluble SnO₂ · xH₂O, is suggested to explain the corrosion protection afforded by alloying with tin. Tin was enriched in the corrosion products while no lead was found. The zinc/copper relation was higher in the corrosion products than in the alloy composition.

Es wird berichtet über die atmosphärische Korrosion von verschiedenen Gußbronzen für Statuen in feuchter Luft mit ppb-Gehalten an SO₂ und SO₂+NO₂. Zusätzlich wurden Kupfer-, Zinn-, Zink- und Blei-Proben in diesen Umgebungen untersucht. Die Proben wurden den synthetischen Atmosphären bei sorgfältiger Kontrolle der Schadgaskonzentrationen, der relativen Feuchtigkeit und der Strömungsbedingungen ausgesetzt. Die Abscheidung von SO₂ wurde mittels on-line Gasanalyse untersucht. Die Gewichtszunahme wurde nach vier Wochen Auslagerung registriert. Die Korrosionsprodukte wurden mit der Elektronenstrahlmikroanalyse (EPMA), der Röntgenbeugung (XRD) und der Fourier-Transformations Infrarot-Spektroskopie (FTIR) analysiert.

Der synergistische Effekt von SO₂ und NO₂ war auf allen untersuchten Bronzen bemerkenswert. Die Gewichtszunahme wurde mit der Legierungszusammensetzung korreliert. Hohe Zink- und niedrige Bleigehalte führten zur größten Gewichtszunahme, während hohe Zinngehalte eine geringe Gewichtszunahme begünstigten. Blei zeigte eine schnelle Abscheidung von SO₂, gefolgt von Zink und Kupfer, während sich Zinn gegenüber SO₂ nicht reaktiv verhielt. Es gab keine Anzeichen, daß das Gefüge die Korrosion beeinflusste.

Die in der SO₂+NO₂ Umgebung gefundene Morphologie der Korrosionsprodukte deutete auf einen örtlichen Angriffstyp. Die anodischen Bereiche waren mit zinnreichen Korrosionsprodukten bedeckt. Es wird vorgeschlagen, den durch das Legieren mit Zinn bewirkten Korrosionsschutz durch die Oxidation von löslichem, zweiwertigen Zinn durch O₂ an den anodischen Bereichen, die zur Bildung von unlöslichem SnO₂ · xH₂O führt, zu erklären. Zinn wurde in den Korrosionsprodukten angereichert, während kein Blei gefunden wurde. Das Zink/Kupfer-Verhältnis war in den Korrosionsprodukten größer als in der Legierung.

1 Introduction

The effect of air pollutants on metals has been the subject of a large number of laboratory investigations and field studies. However, few investigations concern the atmospheric corrosion of copper alloys [1–4]. Holm and Matsson [12] studied the atmospheric corrosion of copper and different bronzes in the field, including up to 16 years long exposures. The authors reported that increasing the tin content in copper alloys tended

to inhibit corrosion on rural sites, while no such effect was noted on the urban and marine sites. In a laboratory investigation in humid SO₂ environments by Bastidas et al. [4], the highest corrosion rate was observed for a copper alloy containing tin, zinc and lead, and the lowest rate was observed for an alloy with tin and lead, but no zinc. Bakaljarova et al. [5] reported tin bronzes to be the most corrosion resistant, followed by pure copper and brass. The microstructure has also been suggested to influence on the corrosion resistance [6–9].

The present work is part of the EURO CARE-COPAL project (EU 316) which aims at investigating the atmospheric corrosion of several copper alloys in diverse environments, the final aim being to develop improved conservation treat-

* H. Strandberg, L.-G. Johansson, O. Lindqvist
Department of Inorganic Chemistry, University of Göteborg,
S-41296 Göteborg (Sweden)

ments for bronze monuments. Within this project some European bronze monuments have been investigated regarding alloy and patina composition [10]. Alloys have been produced for atmospheric corrosion studies with compositions that are representative of some of the monuments included in the project.

The object of this laboratory investigation is to study the atmospheric corrosion of bronzes exposed to humid air containing ppb levels of SO_2 and NO_2 . Different statue bronzes, as well as the pure alloying constituents; copper, tin, zinc and lead, were studied in this respect. The correlation between microstructure and corrosion was investigated as well for one alloy.

The exposures were carried out using a specially developed experimental set-up. Deposition of SO_2 was measured in a time-resolved manner during 20 h exposure; and weight gains of the samples were registered in four-week exposures, followed by analysis of the corrosion products using X-ray diffraction (XRD), Fourier Transform Infrared spectroscopy (FTIR), microscopy, and Electron Probe Micro Analysis (EPMA). A remarkable synergistic effect of SO_2 and NO_2 was found for all bronzes examined. The alloy high in zinc but low in lead exhibited the highest weight gain, while the lowest weight gain was found for the alloy high in tin. Lead exhibited a rapid deposition of SO_2 followed by zinc and copper, while tin was unreactive towards SO_2 . An explanation of the morphology of the corrosion products is attempted based on characterisation of the surface by EPMA.

2 Experimental

2.1 Sample material

Three cast statue bronze alloys of different composition were exposed (Table 1). The Gustav II bronze and the Josef II bronze were produced by the Institut für Silikatchemie und Archäometrie in Vienna, and the commercial bronze was supplied by the Swedish Board of Antiquities in Stockholm. Samples made from the pure alloying constituents, copper, tin, zinc and lead, were also investigated (Cu > 99.85%, Sn 99.9985%, Zn > 99.9%, Pb 99.94%). In the case of the Josef II bronze, material exhibiting two different microstructures was studied, one bronze material being chillcast while the other was tempered. Both materials consisted of α -phase only due to the low tin content (Sn 1.38%).

2.2 Sample preparation

The plates were cut to shape and a hole was drilled in each for suspending the sample by a nylon thread. The samples were polished to 1000 mesh in 99.9% ethanol using SiC paper. The plates were then cleaned in ethanol using ultrasonic

agitation and rinsed before drying at room temperature. The final geometrical area was 15 cm^2 for bronze samples and 20 cm^2 for the pure metals, copper, tin, zinc and lead. The samples were stored in a desiccator over silica gel (<1% RH) for 24 h before the start of the long term corrosion exposures, and for one hour before the deposition experiments.

2.3 Experimental set-up

The experiments were carried out using two different experimental set-ups (Figs. 1 and 2). All equipment was made of glass and Teflon and was immersed in a water tank kept at $22.00 \pm 0.03^\circ\text{C}$. The temperature in the room was kept at $23\text{--}25^\circ\text{C}$ to avoid condensation in the parts of the system outside the water tank. The first part of the system was the same for both experimental set-ups and consisted of an air purification and drying system with particle filters, filters for the absorption of gaseous pollutants, and a self-regenerating air drier based on alumina. The CO_2 content in the purified air was about 200 ppm. The clean and dry air passed into the apparatus by two routes. One air flow passed through the humidifier in which the air was saturated with water vapour at 22.00°C . The other air flow was dry and was used as a carrier for the trace gases. SO_2 and NO_2 was added from thermostated permeation tubes containing the liquefied gas. The total gas flow and the relative humidity were controlled by mixing measured amounts of dry and humidified air.

2.4 Deposition studies

In the apparatus for the short term (20 h) deposition experiments (Fig. 1), a continuous flow of the corrosive humidified air passed through the reaction cell. The sample was suspended by a nylon string, the gas flowing parallel to the sample. Flow conditions were laminar in the cell. The diameter of

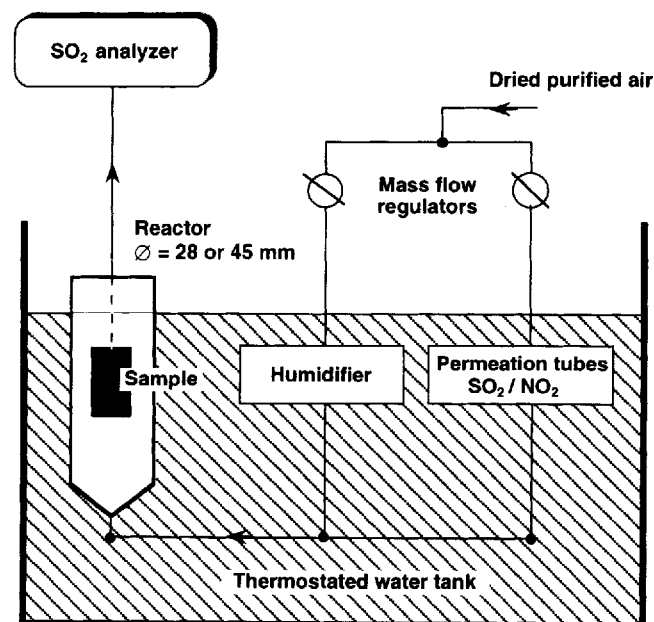


Fig. 1. Experimental set-up for on-line studies of SO_2 -deposition
Abb. 1. Experimenteller Versuchsaufbau für die on-line Untersuchungen der SO_2 -Abscheidung

Table 1. Elemental composition of bronze alloys

Tabelle 1. Zusammensetzung der Bronzelegierungen

Sample	Composition %				
	Cu	Sn	Zn	Pb	Ni
Gustav II Adolf bronze	90.94	5.88	0.63	1.98	0.07
Josef II bronze	92.95	1.38	4.94	0.36	0.07
Commercial bronze	83.55	4.50	5.64	5.51	0.53

the exposure cell was 45 mm in experiments involving the pure metals copper, tin, zinc and lead; and 28 mm in experiments with the bronze samples. The air flow was 1 l/min resulting in a gas velocity of 10.5 and 27.0 mm/s, respectively.

The SO_2 concentration in the gas emanating from the reaction cell was measured continuously using a fluorescence instrument (Environnement AF21M, sensitivity 1 ppb). The deposition rate, defined as the flux of trace gas to the sample surface ($\text{mol}/\text{m}^2\text{ s}$), was determined by comparing input and output concentrations of SO_2 .

2.5 Corrosion studies

The corrosion exposure system used in the four-week exposures is shown in Fig. 2. In this set-up the corrosive humidified gas passed through eight parallel corrosion chambers, each with a volume of 0.4 l and an inner diameter of 55 mm. Each sample was exposed in a chamber of its own. To obtain equal gas flow in all chambers, a multichannel solenoid valve distributed the gas sequentially among the exposure chambers, the whole gas flow passing each chamber in turn for 37.5 seconds. The flow rate was 1 l/min corresponding to a gas velocity of 7 mm/s each time a chamber was open. Flow conditions were laminar in the cell. During the exposures, the samples were removed from the apparatus and weighed regularly. The error in the weighings was estimated to $\pm 40 \mu\text{g}$ corresponding to $\pm 2 \mu\text{g}/\text{cm}^2$. In the SO_2 exposures, weight gains were based on duplicate samples in the case of copper and commercial bronze (largest scatter $\Delta = 5 \mu\text{g}/\text{cm}^2$), while single samples were exposed in the case of Gustav II and Josef II bronze. In the SO_2+NO_2 exposures, two copper samples ($\Delta = 24 \mu\text{g}/\text{cm}^2$), four Josef II bronze samples ($\Delta = 46 \mu\text{g}/\text{cm}^2$), and two commercial bronze samples ($\Delta = 32 \mu\text{g}/\text{cm}^2$) were exposed.

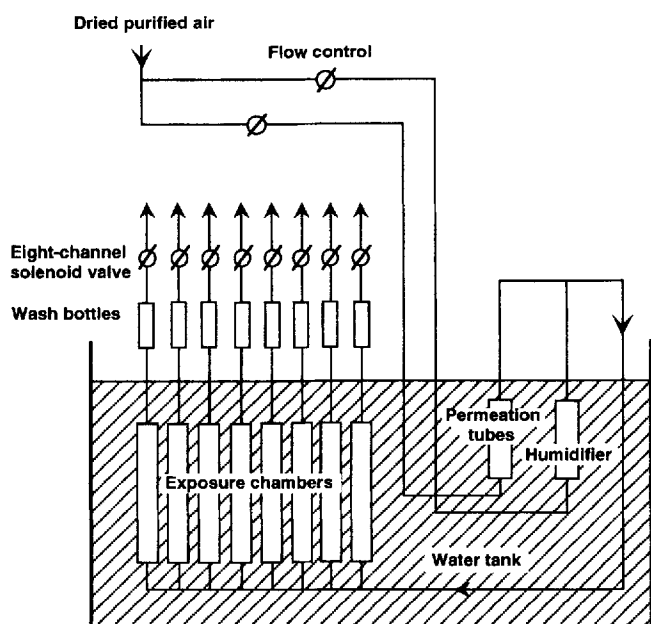


Fig. 2. The corrosion exposure system for studies of atmospheric corrosion in synthetic environments

Abb. 2. Korrosionsauslagerungssystem für Untersuchungen der atmosphärischen Korrosion in synthetischen Umgebungen

2.6 XRD

Crystalline corrosion products were identified by X-ray powder diffraction (XRD) using $\text{Cu K}\alpha_1$ radiation and the Guinier camera technique. Films were evaluated using a computerised photo-scanning system. One lead sample was analysed in a Siemens 5000 θ - θ diffractometer in Bragg-Brentano geometry using the grazing-incidence angle (1.5°) technique.

2.7 FTIR

Infra-red spectra were recorded with a Perkin-Elmer 1800 Fourier Transform Infrared Spectrometer using the KBr disc technique.

2.8 EPMA

Unexposed etched plates and corroded plates were examined with an Electron Probe Micro Analyser (EPMA). Three types of images were displayed. Secondary electron images (SEI) mainly indicated the topography, but was also sensitive to the atomic number. Back scattered electron images (BEI) revealed parts of the surface enriched in elements of high atomic numbers. X-ray mapping was performed to study the distribution of specific elements.

3 Results and discussion

3.1 The interaction of copper, tin, zinc and lead with humid air containing traces of SO_2 and SO_2+NO_2

The deposition of SO_2 on samples made from copper, tin, zinc and lead, i.e., the main constituents of statue bronze, was studied in SO_2 and SO_2+NO_2 environment (500 ppb) at 90% RH (Figs. 3 and 4). Lead interacted most strongly with SO_2 followed by zinc and copper, while tin was unreactive towards SO_2 (Figs. 3 and 4). The presence of NO_2 accelerated the deposition of SO_2 in the case of copper and lead.

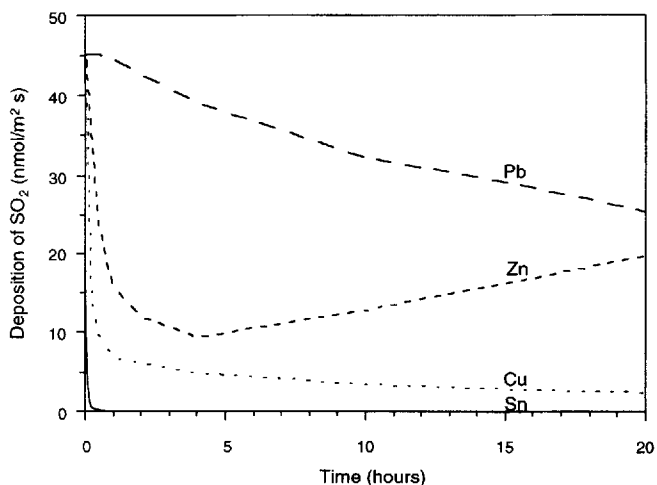


Fig. 3. SO_2 -deposition rate on copper, tin, zinc and lead samples exposed to 500 ppb SO_2 at 90% RH

Abb. 3. SO_2 -Abscheidungsgeschwindigkeit auf Kupfer-, Zinn-, Zink- und Blei-Proben, die 500 ppb SO_2 bei 90% relativer Feuchte ausgesetzt waren

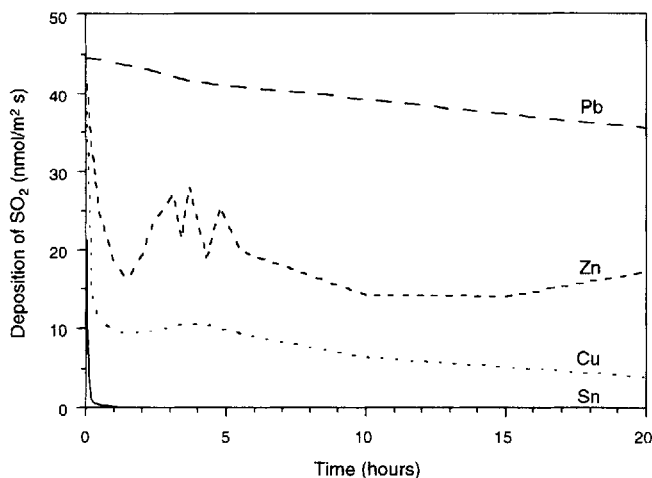


Fig. 4. SO₂-deposition rate on copper, tin, zinc and lead samples exposed to 500 ppb SO₂ and 500 ppb NO₂ at 90% RH

Abb. 4. SO₂-Abscheidungs-geschwindigkeit auf Kupfer-, Zinn-, Zink- und Blei-Proben, die 500 ppb SO₂ und 500 ppb NO₂ bei 90% relativer Feuchte ausgesetzt waren

The interaction of SO₂ on zinc in humid air was investigated by Svensson and Johansson [11]. They reported that SO₂ deposits on the zinc surface to form sparingly soluble zinc sulphite that is subsequently oxidised to soluble zinc sulphate. A rapid corrosion was found at 95% RH, due to an aqueous solution of zinc sulphate forming at humidities above 90% RH. The solid corrosion products formed, mainly zinc hydroxy sulphate and zinc oxide, were suggested to provide new adsorption sites for SO₂, resulting in rapid SO₂ deposition at high humidity. At 70% RH the corrosion of zinc as well as the SO₂ deposition was reported to be slow, due to the lack of electrolyte. In the present study at 90% RH, the deposition rate of SO₂ on zinc passed through a minimum after 3–5 h and then increased slowly (Fig. 3). This behaviour is suggested to reflect the formation of a zinc sulphate electrolyte, and the transfer of zinc into an actively corroding state. The presence of NO₂ did not increase SO₂ deposition appreciably. It may be noted that Svensson and Johansson reported that NO₂ increased the rate of SO₂ deposition at 95% RH, while not at 70% RH. The short duration of the present study at 90% RH, does not allow us to draw conclusions regarding the long-term effect of NO₂, on the SO₂-deposition on zinc.

The deposition of SO₂ on copper was studied previously by Strandberg and Johansson [12], and by Eriksson et al. [13]. The general behaviour is similar to the case of zinc. Thus, cuprite (Cu₂O), sulphite and sulphate were detected after 20 h exposure using FT-IR and XPS. The presence of NO₂ accelerated the corrosion of copper and the deposition of SO₂. This effect was explained by an increased rate of oxidation of sulphite. It was suggested that the acid surface electrolyte thus forming, subsequently attacks the passive film and that an electrochemical corrosion process starts [13]. The SO₂ deposition curves measured in the present investigation (Figs. 3 and 4) are in good agreement with the work cited.

Lead exposed to the atmosphere has been reported to primarily form litharge (PbO) [14]. The reactions occurring initially when lead is exposed to SO₂ are therefore expected to correspond to the reactions of solid PbO. The rapid SO₂ deposition (Figs. 3 and 4) would then be explained by the basic character of PbO. PbO is known to react rapidly with SO₂ and

HSO₄⁻(aq) forming insoluble sulphite and sulphate, respectively [15]. Accordingly, lead has been reported to form a protective layer of anglesite (PbSO₄) when exposed to the outdoor atmosphere [14]. In the present investigation indications for PbSO₃ and lanarkite (Pb₂SO₄O) were found, using grazing angle XRD on lead exposed to air containing SO₂+NO₂ at 90% RH for two weeks. In addition PbO, 3PbO·H₂O and minium (Pb₃O₄) were detected. The presence of NO₂ increased the rate of SO₂ deposition on lead. This effect is suggested to be connected to an increased rate of oxidation of S(IV) species on the metal surface.

Tin was quite unreactive towards SO₂, no deposition being detected after the first hour of exposure. The presence of NO₂ did not increase SO₂ deposition significantly. We assume that the slow reaction is due to the presence of a thin layer of oxide passivating the surface. The oxide may be cassiterite (SnO₂) or, more probably, an amorphous hydrated oxide (SnO₂·xH₂O). Both compounds have acidic character and react slowly or not at all with SO₂ and HSO₄⁻(aq) [16]. An amorphous gel of the hydrated oxide SnO₂·xH₂O has been suggested to form on bronzes exposed in outdoor environments [8].

3.2 The atmospheric corrosion of statue bronze in humid air containing SO₂ and SO₂+NO₂

The corrosion of statue bronze in air containing traces of SO₂ and SO₂+NO₂ was studied at 90% RH (Figs. 5 and 6). The composition of the sample material is presented in Table 1. Copper was included in the exposure for reference. The corrosion process was studied by measuring SO₂ deposition during the first 20 h of exposure, by recording the weight gain during the four week exposures, by investigating the morphology and composition of the corrosion products, and by visual inspection of samples.

Commercial bronze exhibited the highest deposition rate of SO₂ after 20 h exposure, followed by the Josef II bronze and the Gustav II Adolf bronze, the deposition on copper being slowest (Fig. 5 and 6).

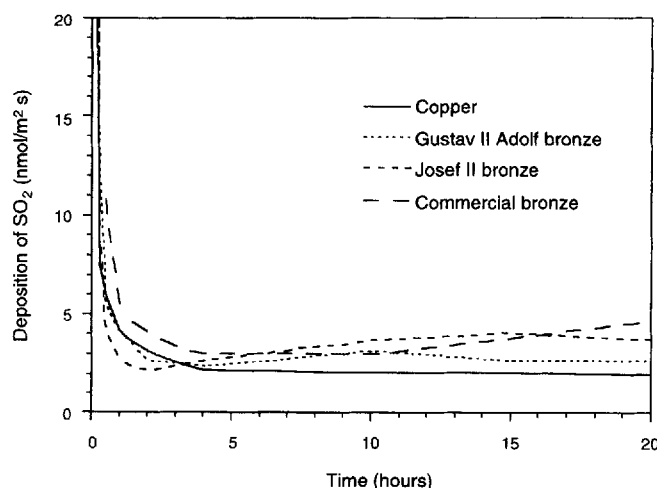


Fig. 5. SO₂-deposition rate on bronze samples exposed to 500 ppb SO₂ at 90% RH

Abb. 5. SO₂-Abscheidungs-geschwindigkeit auf Bronze-Proben, die 500 ppb SO₂ bei 90% relativer Feuchte ausgesetzt waren

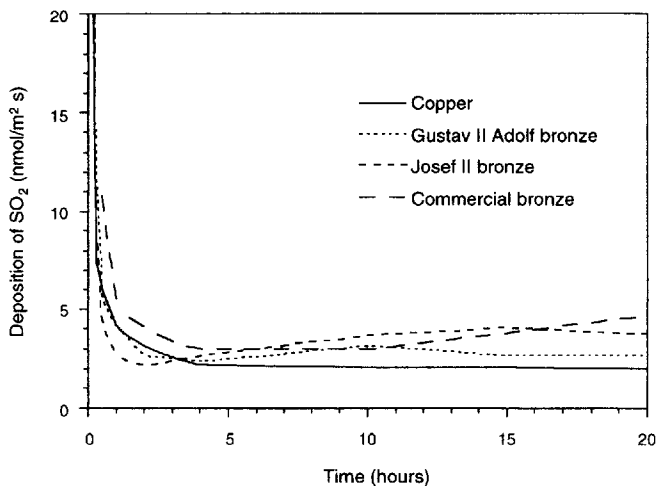


Fig. 6. SO_2 -deposition rate on bronze samples exposed to 500 ppb SO_2 and 500 ppb NO_2 at 90% RH

Abb. 6. SO_2 -Abscheidungs-geschwindigkeit auf Bronze-Proben, die 500 ppb SO_2 und 500 ppb NO_2 bei 90% relativer Feuchte ausgesetzt waren

Samples exposed to SO_2 in the absence of NO_2 , exhibited a slow but steady weight gain (Figure 7). The visual appearance remained golden lustrous but deepened in tone during exposure. However, the Josef II bronze and the commercial bronze samples developed some dull spots at an early stage. After four weeks exposure the Josef II bronze exhibited the highest weight gain of the alloys, followed by commercial bronze and Gustav II Adolf bronze.

The presence of NO_2 resulted in an increased rate of SO_2 -deposition (compare Figs. 5 and 6). The synergistic effect of SO_2 and NO_2 was remarkable, the weight gain after four weeks increasing 10–20 times in the presence of NO_2 (Fig. 7). The largest weight gain was registered for the Josef II

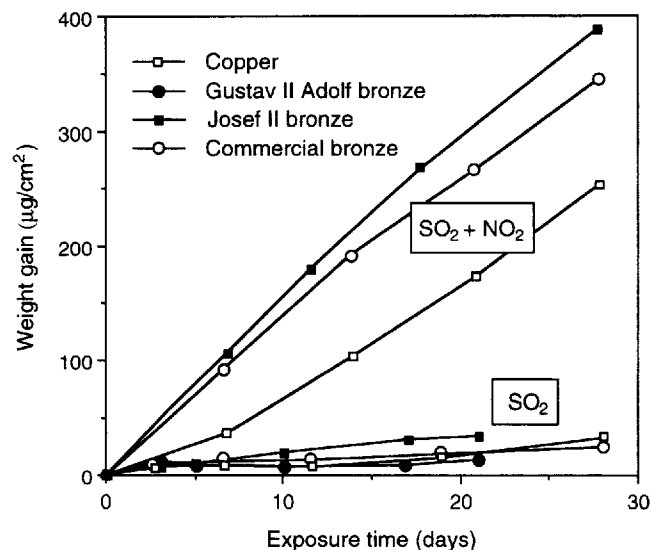


Fig. 7. Weight gain of bronze samples exposed at 90% RH to 500 ppb SO_2 , or to 500 ppb SO_2 and 500 ppb NO_2

Abb. 7. Gewichtszunahme von Bronze-Proben, die bei 90% relativer Feuchte 500 ppb SO_2 oder 500 ppb SO_2 und 500 ppb NO_2 ausgesetzt waren

bronze followed by commercial bronze and copper. After exposure the samples appeared dull greyish brown with green spots.

Cuprite (Cu_2O) was detected on all samples by XRD, being most abundant on the samples exposed to SO_2 and NO_2 . $\text{Cu}_{2.5}(\text{OH})_3\text{SO}_4 \cdot 2\text{H}_2\text{O}$, a recently described corrosion product of copper [17], was also identified on all samples. These results were corroborated by FTIR spectroscopy of the corrosion products showing peaks corresponding to cuprite ($\sim 620 \text{ cm}^{-1}$) and to sulphate ($\sim 1100 \text{ cm}^{-1}$). Analysing samples exposed in atmospheres containing NO_2 , weak peaks indicating the presence of nitrate ($\sim 1380 \text{ cm}^{-1}$) were found.

The weight gain after four weeks exposure tended to be greatest for the alloys with the highest zinc content (Fig. 7). This is in agreement with previous studies [4, 5] reporting a reduction in the corrosion resistance with increasing zinc content in the alloy. The deposition of SO_2 tended to increase with the lead and zinc content of the alloys (Figs. 5 and 6). This behaviour is in accordance with the results obtained for the pure metals (Figs. 3 and 4).

The addition of tin has long been used to enhance the corrosion resistance of copper alloys [9]. A corrosion-inhibitive effect of tin was indicated in a field study in mildly corrosive conditions [2]. Amorphous hydrated tin oxide, $\text{SnO}_2 \cdot x\text{H}_2\text{O}$, is assumed to form a protecting barrier on the bronze surface [8]. However, this film has not been fully characterised. The amount of tin in bronzes has also been shown to determine the corrosion rate in sea water [9]. In accordance with these previous results, the lowest weight increase in the present study was registered for the bronze with the highest amount of tin (see Fig. 7). Thus, tin may indeed have a passivating effect in the environments studied.

The strong synergistic effect of the combination of SO_2 and NO_2 on the corrosion rate of bronze found in the present study is reminiscent of the behaviour of pure copper reported by Eriksson et al. [13]. In the case of copper the synergistic effect was attributed to an enhanced rate of oxidation of sulphite to sulphate in the presence of NO_2 . The acidic sulphate electrolyte formed was suggested to destroy the protective oxide film, resulting in an electrochemical corrosion process. It is suggested that the behaviour of bronze may be explained along similar lines. Evidence was also found for an electrochemical corrosion process occurring on Josef II bronze in $\text{SO}_2 + \text{NO}_2$ environment (see section 3.4).

3.3 Influence of microstructure on the atmospheric corrosion of bronze

The microstructure of a bronze may differ due to varying cooling rate in different parts of the casting. When the metal initially hits the cold mould, it forms a fine-grained homogeneous layer, termed a chilled layer. As solidification continues, larger crystal dendrites are formed in the body of the casting [6]. Copper is enriched in parts where the alloy solidifies first, while tin and lead are enriched in the areas that solidifies last [18]. Porosity in the bronze is caused by gas evolved during solidification.

A cast bronze thus exhibits areas of different microstructure that may have different susceptibility to corrosion. A faster corrosion rate have been observed where pieces of the mould have been joined on sculptures [6]. This may be due to differences in microstructure, but also to differences in composition. Patterns of "black islands" and light green pits on outdoor weathered bronzes, have also been suggested to be re-

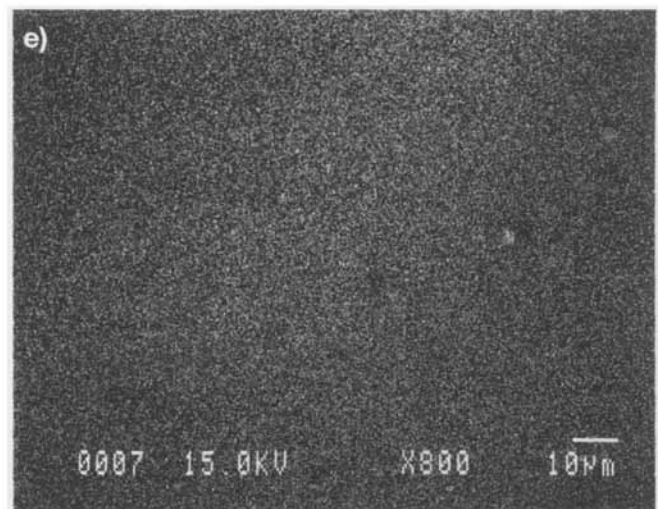
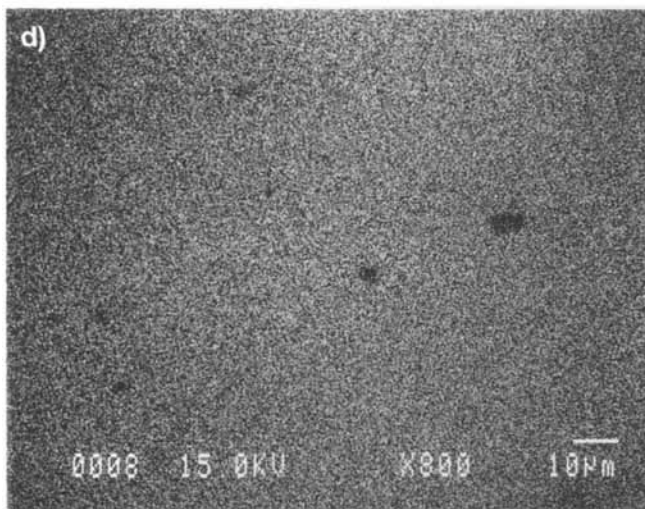
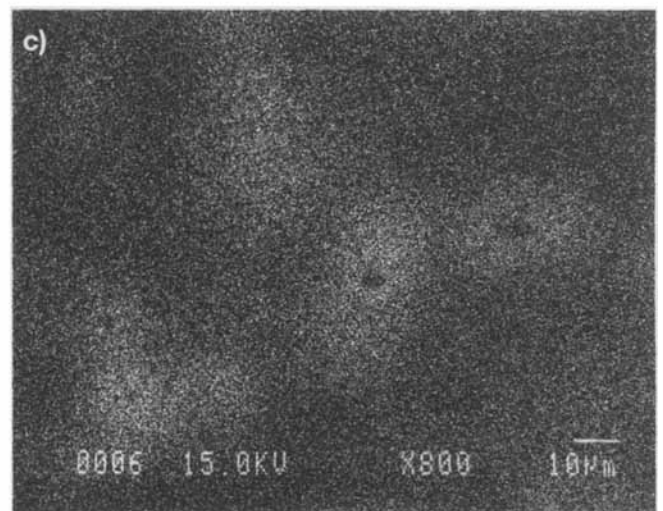
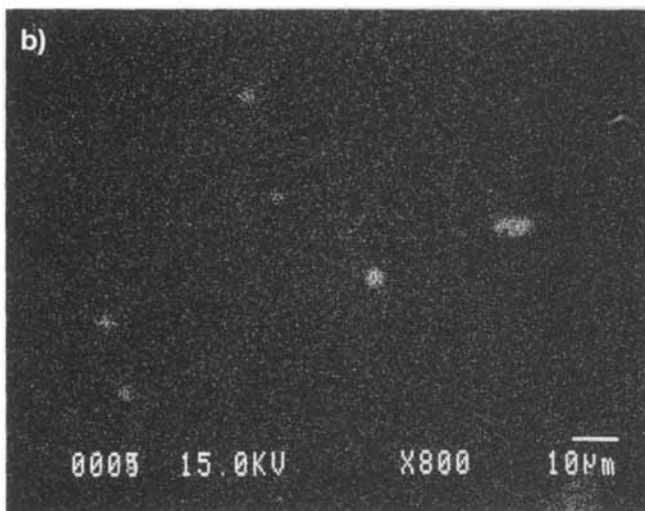
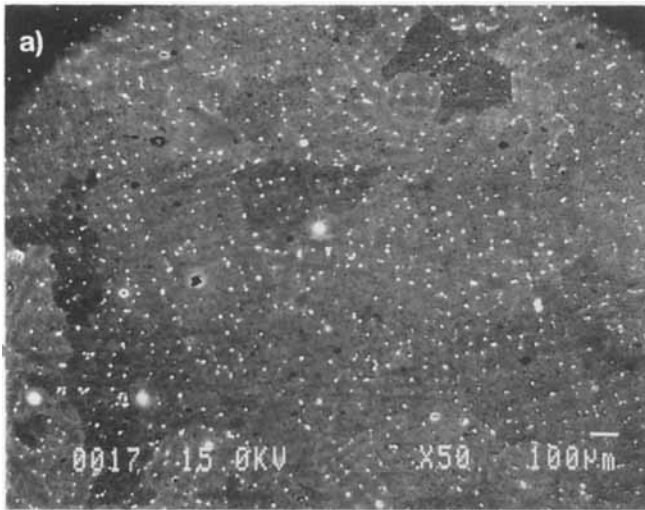


Fig. 8. Chillcast plate after etching (EPMA). a) The dendritic structure contains a phase of higher atomic number apparent as white dots (BEI image). Typical grain sizes are about 0.2 mm. b) Lead in the center of the remaining melt (X-ray mapping of Pb). c) A higher concentration of tin in the remaining melt (X-ray mapping of Sn). d) Copper is lacking where lead is present (X-ray mapping of Cu). e) Zinc is evenly distributed (X-ray mapping of Zn)

Abb. 8. Hartgußplatte nach dem Ätzen (EPMA). a) Das dendritische Gefüge enthält eine Phase höherer Atomzahl, sichtbar an den weißen Punkten (BEI image). Typische Korngröße ist etwa 0,2 mm. b) Blei ist im Zentrum der Restschmelze (X-ray mapping von Pb). c) In der Restschmelze ist eine höhere Zinnkonzentration (X-ray mapping von Sn). d) Kupfer mangelt dort, wo Blei vorhanden ist (X-ray mapping von Cu). e) Zink ist gleichmäßig verteilt (X-ray mapping von Zn)

lated to microsegregations in the alloy [8]. A copper-rich α -phase has been reported to corrode preferentially compared to a tin-rich δ -phase, in outdoor atmosphere [7] as well as under marine conditions [9]. Moreover, a chillcast structure has been proposed to resist corrosion better than a coarse-grained structure [6]. On the other hand no distinct relation between metallographic structure and corrosion rate was found on some outdoor sculptures [19].

In the present investigation the correlation between microstructure and atmospheric corrosion was studied. Two cast materials of the Josef II bronze (92.95% Cu, 1.38% Sn, 4.94% Zn and 0.36% Pb) were studied, one being chillcast (fast cooling) and the other being tempered (slow cooling). Samples were exposed in air containing SO_2 and NO_2 at 90% RH, for 20 h (deposition studies) or in four weeks (corrosion studies).

The microstructures were examined by microscopy after polishing and etching unexposed samples in a mixture of 30% H_2O_2 , conc. $\text{NH}_3(\text{aq})$ and H_2O (2:5:5). The grains

were smaller in the chillcast material compared to the tempered material (0.2 mm and 0.4 mm average grain diameter, respectively, Figs. 8a and 9a). Both microstructures were segregated, but only consisted of an α solid solution as the tin-content was low (1.38%). In the chillcast structure, the space between the dendrites was enriched in tin and contained globules of lead (Figs. 8b, c). The tempered material exhibited lead and tin concentrated at the grain boundaries (Figs. 9b, c). Zinc was evenly distributed in both microstructures (Fig. 8e). The tempered material was less homogenous regarding grain size and lead content.

No significant correlation between microstructure and weight gain or SO_2 deposition was found for the materials investigated. However, the tempered samples showed more scattering in the weight gain results ($\Delta = 50 \mu\text{g}/\text{cm}^2$) compared to the chillcast plates ($\Delta = 20 \mu\text{g}/\text{cm}^2$), possibly due to the material being less homogeneous. The corroded surface did not reflect the microstructure of the metal when examined by microscopy and EPMA after four weeks exposure.

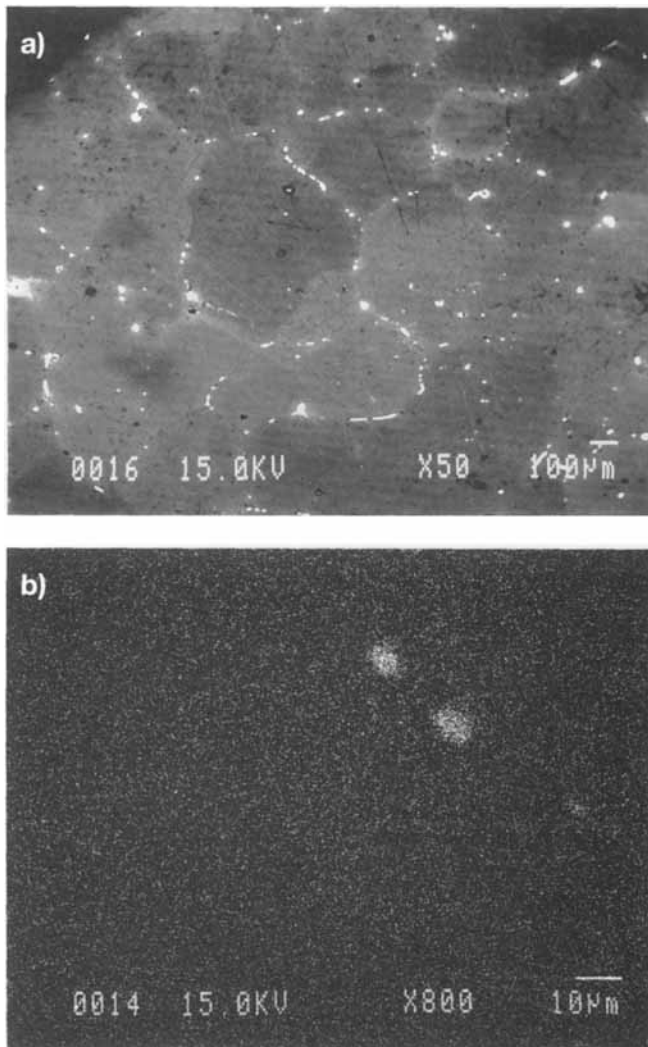


Fig. 9. Tempered plate after etching (EPMA). a) Grains have typical sizes of about 0.4 mm. A phase of higher atomic number is mainly enriched in the grain boundaries (BEI image). b) Lead at the grain boundary (X-ray mapping of Pb). c) Tin is higher in the vicinity of the grain boundary (X-ray mapping of Sn).

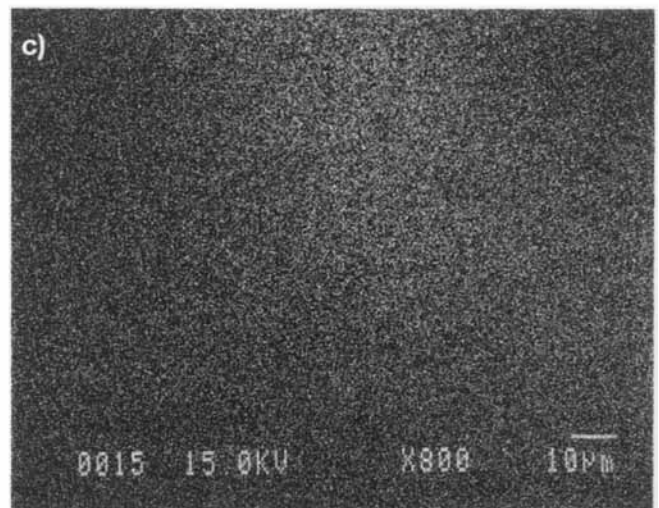


Abb. 9. Angelassene Platte nach dem Ätzen (EPMA). a) Die Körner haben eine typische Größe von etwa 0,4 mm. Eine Phase höherer Atomzahl ist im wesentlichen an den Korngrenzen angereichert (BEI image). b) Blei ist an den Korngrenzen (X-ray mapping von Pb). c) Die Zinnkonzentration ist in der Nähe der Korngrenze höher (X-ray mapping von Sn)

Table 2. Elemental distribution in corrosion products of Josef II bronze examined by EPMA. The amounts of different elements in relation to the bare metal surface (region 1) is presented for the four characteristic regions**Tabelle 2.** Mittels EPMA ermittelte Elementverteilung in den Korrosionsprodukten der Josef II Bronze. Die Menge der verschiedenen Elemente ist für die vier charakteristischen Bereiche in Relation zur blanken Metalloberfläche (Bereich 1) angegeben

Region	Pb	Sn	Zn	Cu	S
1. Bare metal surface where corrosion layer is lacking	n.d.	0	0	0	0
2. Thin corrosion layer inbetween the outgrowths	n.d.	0	0	–	+
3. Outgrowth	n.d.	–	0	– –	++
4. Tin-rich layer beneath the outgrowths	n.d.	++	0	– –	0

Images of the corroded surface are shown only for the chillcast plate (Figs. 10a–f). Corrosion product characterisation with FTIR and XRD also showed identical results for the two materials. The only noticeable effect of microstructure on corrosion was the visual appearance of the sample. After one week the chillcast plates developed a dark grainy and continuous patina, while the tempered plates were still golden in parts, with dark stains and a cracked pattern. At the end of the exposure, the chillcast plates exhibited greenish and reddish nuances while the tempered plates were greyer.

3.4 The atmospheric corrosion of a statue bronze studied by EPMA

A corroded bronze sample (Josef II bronze) was studied using EPMA, after four weeks exposure in humid air containing SO₂ and NO₂. The corroded metal surface exhibited flower-like outgrowths of corrosion products (Fig. 10a). Between these outgrowths the corrosion products formed a thin, even layer. The surface can be described in terms of four characteristic regions depicted in Table 2. The X-ray mapping in Figures 10b–f shows the distribution of elements in these areas seen from above, while mapping of the cross-section (Fig. 11) is not presented in this paper.

Beneath the outgrowths, close to the metal, a thin layer (about 1 μm) was found as shown in the cross-section in Figure 11. This layer was rich in tin and low in sulphur. X-ray mapping of the surface showed that the outgrowths were high in sulphur and low in tin. At the centre of the outgrowths the tin-rich bottom layer was visible (Figs. 10c, f). Thus, the flower-like outgrowths, featuring a hole at the centre, and containing sulphur and zinc with some copper, had formed on top of the tin-rich layer. The dark area beneath the tin-rich layer shown in Figure 11 indicates that the layer had flaked, probably during dry storage. The rough corroded metal surface is revealed underneath.

The thin, adherent corrosion product layer covering much of the surface, contained sulphur and was somewhat depleted in copper compared to the metal surface (Figs. 10e, f). This layer is seen as the smooth adherent layer to the right in the cross-section (Fig. 11).

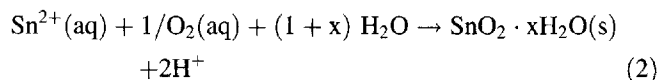
It is proposed that the corrosion product morphology produced in SO₂+NO₂ environment can be interpreted in terms of a localised type of attack. The centres of the outgrowths are suggested to correspond to sites of anodic dissolution of metal. There is no indication that certain elements are enriched, in the underlying alloy at these sites, moreover there is no cor-

relation to microstructure. We suggest that the flower-like outgrowth results from the migration of cations from the anodic site at the centre towards cathodic areas at the periphery.

The enrichment of tin in the corrosion products closest to the metal is suggested to be explained by the redox-chemistry of tin. Metallic tin is known to dissolve as divalent ions:



However, divalent tin in aqueous solution readily reacts with oxygen molecules to form tetravalent tin:



Sn(IV) precipitates as a hydrated oxide (SnO₂ · xH₂O) that is quite insoluble in neutral media. Thus, tin in divalent soluble form is expected to be stable only in reducing conditions, i.e. close to the metal, while it is expected to precipitate as SnO₂ · xH₂O when oxidised by O₂. This explains why tin is usually found to be enriched at the bottom of the corrosion product layer, closest to the metal. In contrast, copper and zinc form more soluble corrosion products and may migrate towards the cathodic sites at the periphery of the outgrowths. We suggest that the amorphous tin oxide gel, covering the anodic sites, tends to slow down the rate of metal dissolution, explaining the corrosion protection afforded by tin alloying.

In accordance with the observations made in the present study, tin was reported to be enriched in the corrosion products on copper-tin alloys in outdoor conditions [8]. Moreover, insoluble tin compounds were observed in the inner regions of corrosion product layers [8]. In a field study of bronze monuments in outdoor environments there was no indication that zinc was preferentially removed by runoff from the bronze [20]. In this study, however, zinc was found to be enriched in the corrosion products. The zinc/copper relation was higher in the corrosion products than in the alloy composition.

4 Conclusions

The synergistic effect of SO₂ and NO₂ was remarkable for all bronze alloys examined, the weight gain in humid air containing traces of SO₂ increasing 10–20 times when NO₂ was present.

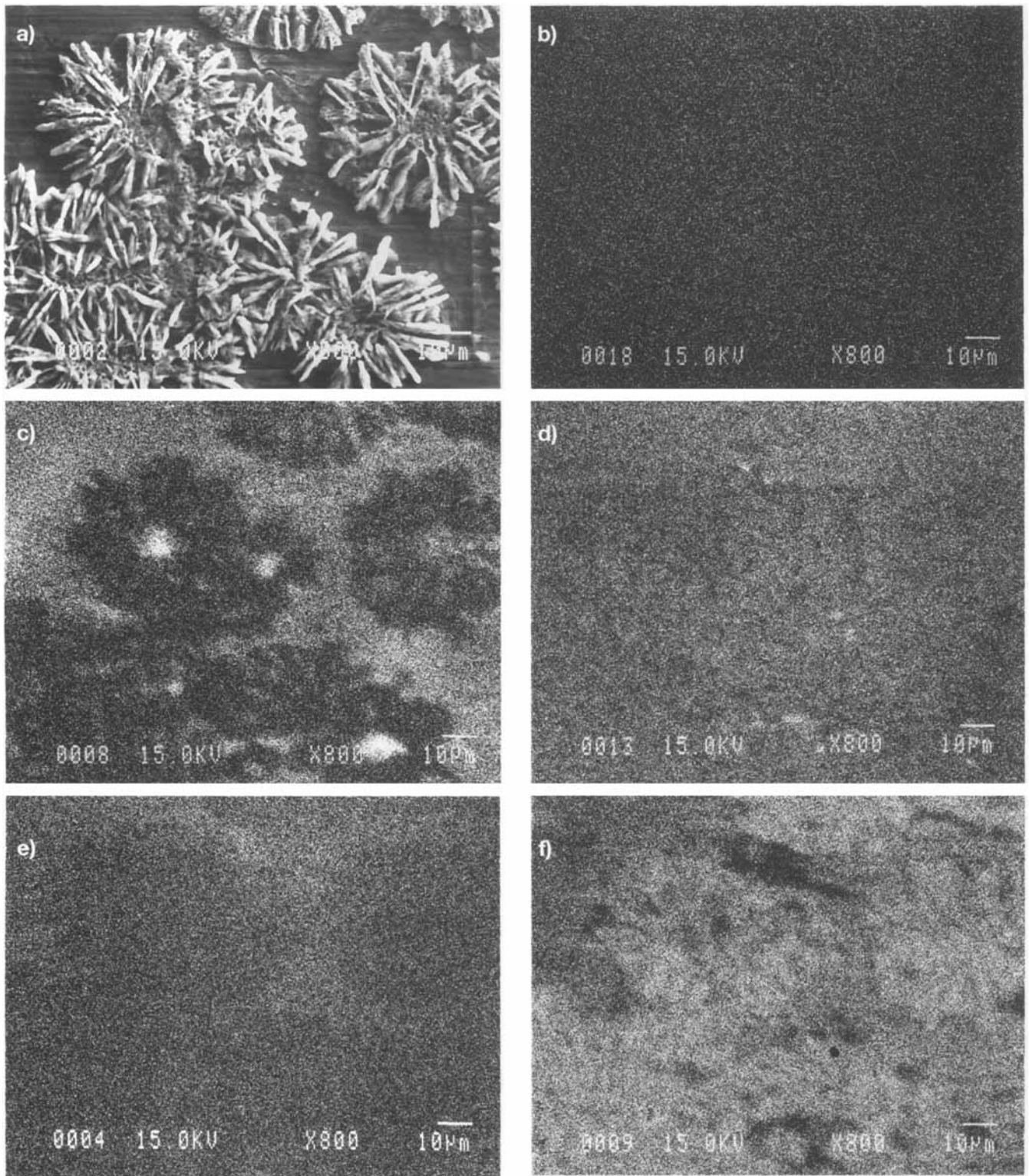


Fig. 10. The chillcast plate after exposure to 500 ppb SO_2 and 500 ppb NO_2 at 90% RH (EPMA). a) Corrosion products are forming flower-like outgrowths on a surface covered with a thin corrosion layer (SEI image). b) There are no signs of lead in the corrosion products (X-ray mapping of Pb). c) Tin is lacking in the outgrowths but is high in the center (X-ray mapping of Sn). d) Zinc is quite evenly distributed. However, small areas of higher zinc content are visible (X-ray mapping of Zn). e) Copper is highest in concentration where the corrosion layer is lacking (small area in upper part) and lowest in the outgrowths (X-ray mapping of Cu). f) Sulphur is most abundant in the outgrowths but is also present in the thin corrosion layer (X-ray mapping of S) and is lacking in the center of the outgrowths

Abb. 10. Die Hartgußplatte nach Auslagerung bei 500 ppb SO_2 und 500 ppb NO_2 , 90% relativer Feuchte (EPMA). a) Die Korrosionsprodukte bilden blumenartige Auswüchse auf einer mit einer dünnen Korrosionsschicht bedeckten Oberfläche (SEI image). b) Es gibt keine Anzeichen von Blei in den Korrosionsprodukten (X-ray mapping von Pb). c) Zinn fehlt in den Auswüchsen, ist jedoch in der Mitte vorhanden (X-ray mapping von Sn). d) Zink ist relativ gleichmäßig verteilt. Es sind jedoch kleine Bereiche mit höherem Zinkgehalt sichtbar (X-ray mapping von Zn). e) Die Kupferkonzentration ist dort am höchsten, wo keine Korrosionsschicht vorhanden ist (kleiner Bereich im oberen Teil) und am niedrigsten in den Auswüchsen (X-ray mapping von Cu). f) Schwefel ist in den Auswüchsen reichlich vorhanden, ist aber auch in der dünnen Korrosionsschicht vorhanden und fehlt in der Mitte der Auswüchse (X-ray mapping von S)

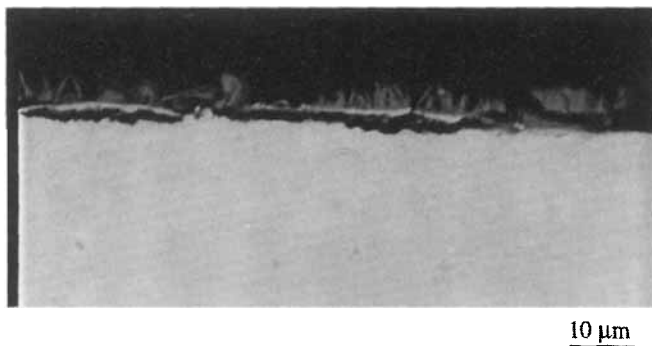


Fig. 11. Cross section of the chillcast plate after exposure to 500 ppb SO₂ and 500 ppb NO₂ at 90% RH (EPMA, BEI image). The corrosion layer has flaked from the metal in some parts

Abb. 11. Querschliff durch die Hartgußplatte nach Auslagerung bei 500 ppb SO₂ und 500 ppb NO₂, 90% relativer Feuchte (EPMA, BEI image). Die Korrosionsschicht ist an einigen Stellen vom Metall abgeplatzt

The alloy high in zinc and low in lead exhibited the greatest weight gain, while high tin content resulted in a low weight increase.

There was no indication that microstructure influenced the corrosion of the alloy studied. However, there was a slight difference in the visual appearance of the chillcast and tempered material in course of the exposure.

The corrosion product morphology found in SO₂+NO₂ environment, was interpreted in terms of a localised type of attack. The anodic sites were covered by a tin-rich corrosion product close to the metal. More soluble zinc, copper, and sulphur-rich corrosion products formed flower-like outgrowths, on top of this layer. The enrichment of tin at the bottom of the corrosion product layer, was explained by the oxidation of soluble divalent tin by O₂ to form insoluble SnO₂ · xH₂O. The decreased corrosion rate exhibited by copper alloys containing tin, is suggested to be connected to the precipitation of SnO₂ · xH₂O on anodic sites.

5 Acknowledgements

This present work was partly financed by the Swedish National Board for Industrial and Technical Development (NUTEK). The authors would like to express their gratitude to "Institut für Silikatchemie und Archäometrie" in Vienna and the Swedish Board of Antiquities in Stockholm for supplying the bronze material.

6 References

- [1] *J. Riederer*: Werkstoffe und Korrosion 23 (1972) 1097.
- [2] *R. Holm, E. Mattsson*: in Atmospheric Corrosion of Metals, ASTM STP 767, Eds. S. W. Dean, Jr., E. C. Rhea., American Society for Testing and Materials (1982) p. 85.
- [3] *P. Eriksson, L.-G. Johansson, J. Gullman*: Corrosion Science 34 (1993) 1083.
- [4] *J. M. Bastidas, M. P. Alonso, E. M. Mora, B. Chico*: Materials and Corrosion 46 (1995) 515.
- [5] *E. Bakaliarova, N. Timofeeva, M. Kalich, I. Kassatonova*: ICOM Committee for Conservation, 9th Triennial Meeting, Conference Preprints, Dresden (1990) Vol. II, p. 711.
- [6] *V. N. Naudé (Ed.)*: in Proc. Sculptural monuments in an outdoor environment, Philadelphia, November 1983, Pennsylvania Academy of Fine Arts, Philadelphia PA (1983), pp. 78–82.
- [7] *A. Lins*: in Dialogue/89-, in Proc. The conservation of bronze sculpture in the outdoor environment: A dialogue among conservators, curators, environmental scientists, and corrosion engineers. Houston, Texas 1989, Ed. T. Drayman-Weisser, NACE (National Association of Corrosion Engineers), (1992), p. 209.
- [8] *L. Robbiola, C. Fiaud, S. Pennec*: in ICOM Committee for Conservation 10th Triennial Meeting, Conference Preprints, Washington (1993), Vol. II, p. 796.
- [9] *I. D. MacLeod, S. Pennec*: ICOM Committee for Conservation, 9th Triennial Meeting, Conference Preprints, Dresden (1990), Vol. II, p. 732.
- [10] *Eurocare-Copal (EU 316)*: Workshop in Budapest, 1994-May-09, Institut für Silikatchemie und Archäometrie, Vienna (1994). Unpublished report.
- [11] *J.-E. Svensson, L.-G. Johansson*: J. Electrochem. Soc., 140 (1993) 2210.
- [12] *H. Strandberg, L.-G. Johansson*: J. Electrochem. Soc., 144 (1997) 81.
- [13] *P. Eriksson, L.-G. Johansson, H. Strandberg*: J. Electrochem. Soc., 140 (1993) 53.
- [14] *T. E. Graedel*: J. Electrochem. Soc., 141 (1994) 922.
- [15] *Gmelin*: Blei, in Gmelins Handbuch der Anorganischen Chemie (1969) Verlag Chemie, GmbH., Weinheim, Bergstrasse, System Nr. 47, Teil C2, p. 535.
- [16] *Gmelin*: Zinn, in Gmelins Handbuch der Anorganischen Chemie (1972) Verlag Chemie, GmbH., Weinheim, Bergstrasse, System Nr. 46, Teil C1, p. 112.
- [17] *H. Strandberg, V. Langer, G. Johansson*: Acta Chem. Scand. 49 (1995) 5.
- [18] *N. Ammannati, E. Martellucci, G. Mei*: in Verrocchio's Christ and St. Thomas – a masterpiece of sculpture from renaissance Florence, Ed. L. Dolcini, The Metropolitan Museum of Art, New York (1992) p. 110.
- [19] *J. Gullman, M. Törnblom*: Bronze sculpture – Its making and unmaking, Central Board of National Antiquities: Stockholm (1994) p. 140.
- [20] *J. D. Meakin, D. Ames, D. A. Dolske*, Atm. Environ., Vol. 26 B, (1992) p. 207.

(Received: February 17, 1997)

W 3194